AIAA JOURNAL
Vol. 35, No. 10, October 1997

Mach Wave Elimination in Supersonic Jets

Dimitri Papamoschou*
University of California, Irvine, Irvine, California 92717-3975

Experimental results are presented on a method that eliminates Mach waves from the exhaust of supersonic jets and, hence, that removes a strong component of supersonic jet noise. Elimination is achieved by surrounding the jet with an annular stream at prescribed velocity and temperature so that all turbulent motions become intrinsically subsonic. No mechanical suppressors are used. Implementation of the technique in a typical turbofan engine is estimated to increase takeoff thrust with minimal impact on overall fuel consumption.

I. Introduction

COMMUNITY noise is one of the major technological hurdles facing future supersonic transports, such as the high-speed civil transport (HSCT). The hot supersonic jets exhausting from the engines of such aircraft are powerful noise generators, especially during takeoff. Untreated, they create noise levels that are environmentally unacceptable. Numerous theoretical, computational, and experimental studies have attributed the elevated noise to Mach waves, which are pressure waves generated by the supersonic motion of turbulent eddies with respect to the surrounding air. Noted here are some key works in the field. Experiments of McLaughlin et al.,[1] followed by those of Troutt and McLaughlin,[2] established that sound is amplified in a direction consistent with the propagation of Mach waves (directivity of sound). Tam and Burton[3] used linear stability theory to accurately predict the sound produced by Mach wave radiation from a cold round jet. Their analysis was extended to hot jets by Tam et al.[4] and by Seiner et al.[5] Most recently, Mitchell et al.[6] performed direct numerical simulation of round jets and found that the near and far fields of supersonic jets are much noisier than those of subsonic jets, again due to intense Mach wave radiation. In addition to Mach wave noise, screech becomes dominant in jets with strong shocks, i.e., in under- or overexpanded jets. The current study focuses on perfectly expanded jets, which do not produce screech noise.

To reduce Mach wave emission, two approaches are now predominant: mixing enhancement, usually via lobe mixers, and ejector shrouds.[7] Often, the two methods are combined. Mixing enhancement reduces the length of the Mach wave emitting region of the jet. It does so with the risk of amplifying near-field Mach waves and with appreciable thrust penalties. For example, in the work of Nagamatsu et al.,[8] each decibel of noise reduction was accompanied by 1% thrust loss. For 10-dB noise reduction, the thrust loss would be 10%, which is unacceptably high. Ejector shrouds encase the jet until it decelerates to sonic or subsonic speeds; thus, most or all of the Mach wave radiation is confined internally. Ejectors provide some thrust augmentation at low flight Mach numbers but penalize thrust at Mach numbers higher than about 0.6 (Ref. 9). Hence, ejectors may need to be retractable, adding to the complexity and weight of the system. There has been significant progress on combination of lobe mixers with ejectors.[10] Current suppression concepts revolve around such combinations, but thrust and weight penalties remain serious concerns.

Other schemes to reduce noise have included the inverted velocity profile (IVP) and the thermal acoustic shield (TAS), overviewed by Seiner and Krejsa.[7] The advantage of IVP coannular jets, as opposed to jets with normal velocity profile (NVP), is faster mixing due to increased contact area with the surrounding fluid. Tanna[11] compared NVP with IVP jets at equal thrust and mass flow rate and concluded that IVP jets are quieter in terms of overall sound pressure level but noisier in terms of perceived noise level. His work was limited to high-subsonic jet velocities and, thus, may not be directly applicable to supersonic jets. Dosanjh et al.[12] investigated coannular supersonic jets with inverted velocity profile and observed significant noise reduction at certain combinations of pressure ratios for the inner and outer streams. Their noise reduction came primarily from minimization of the shock structure internal to the jet, not suppression of Mach wave radiation. The TAS method uses a refractive layer of gas, located at a certain distance from the nozzle lip, that surrounds the engine exhaust. The layer partially reflects the acoustic radiation emitted by the jet and provides good noise reduction for static conditions. At forward flight, however, the layer dissipates quickly and so does the acoustic benefit.

The present technique shares an external similarity with the IVP and TAS in that it utilizes an outer stream that surrounds the inner jet core. However, it is substantially different from the IVP and TAS in its nature and implementation. The IVP and TAS did not address Mach wave radiation explicitly and, therefore, did not provide guidelines for its suppression or elimination. Use of an outer stream creates a reduction in the mean shear experienced by the inner stream, leading to some reduction of the noise produced by that stream. However, as will be seen, Mach wave suppression entails a special range of flow conditions for the outer stream and certain geometric conditions for the nozzles. The TAS, as implemented in Ref. 13, does not meet the geometric requirements, and it is uncertain if it satisfies the flow conditions. The IVP meets the geometric conditions but violates the flow requirements: it is anticipated to reduce Mach wave emission from the inner stream but exacerbate radiation from the outer stream. Thus, the technique presented here is believed to be distinct from the earlier methods. It utilizes propulsive means to prevent generation of Mach waves, in contrast to the prevailing methods, which use mechanical devices or acoustic shields to suppress Mach waves after they are formed. It is expected to perform well at static and forward-flight conditions, in contrast to the TAS, which worked satisfactorily only at very low flight speeds. To the knowledge of the author, the experiments described here are the first to demonstrate the capabilities of this new approach.

II. Mach Wave Elimination

Mach waves, a dominant source of supersonic jet noise, are generated because turbulent eddies in the jet propagate with a convective velocity U_c, which is supersonic with respect to the surrounding airstream, as shown in Fig. 1. Measurements of convective velocity in supersonic–subsonic shear layers, like those surrounding the potential core of the jet, have shown that U_c approaches 80–90% of the velocity of the fast stream.[14–16] This is consistent with the slope of Mach waves emitted from supersonic jets or shear layers, observed by many investigators (see, for example, Refs. 16 and 17).

The principle of Mach wave elimination (Fig. 2) is to surround the jet exhaust with a layer of coflowing gas whose properties are tailored such that 1) the jet eddies become subsonic with respect to the coflow and 2) the coflow eddies are subsonic with respect to the ambient airstream. Because all eddy motions are subsonic with

Received Jan. 16, 1997; revision received July 7, 1997; accepted for publication July 16, 1997.

*Associate Professor, Department of Mechanical and Aerospace Engineering. E-mail: dpapamos@uci.edu. Member AIAA.

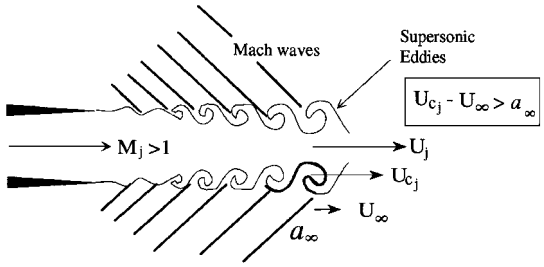

Fig. 1 Mach wave radiation in a supersonic jet.

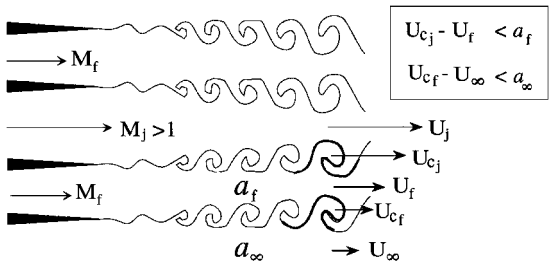

Fig. 2 Principle of Mach wave elimination: creation of coflow adjacent to main jet so that all eddy motions become intrinsically subsonic.

respect to their surrounding streams, no Mach waves are generated. In the analysis that follows, subscript j denotes the jet properties, f the coflow properties, and ∞ the ambient airstream properties. The symbol U represents the flow velocity, a the speed of sound, $M = U/a$ the Mach number, and U_c the convective velocity of the eddies.

Thus, to prevent generation of Mach waves, we must satisfy

$$U_{cj} - U_f < a_f \tag{1}$$

and

$$U_{cf} - U_\infty < a_\infty \tag{2}$$

These relations can also be cast in terms of the convective Mach number of the eddy with respect to the low-speed side, commonly referred to as M_{c2}. Here, we require $M_{c2_j} < 1$ and $M_{c2_f} < 1$.

To translate these requirements into practical guidelines for the coflow properties, we use recent experimental data on the convective velocity U_c in planar shear layers between a supersonic stream (subscript 1) and a subsonic stream (subscript 2). Papamoschou and Bunyajitradulya[18] used planar laser-induced fluorescence in a double-exposure setup to obtain direct measurements of U_c and, hence, of the convective Mach numbers M_{c1} and M_{c2}. Two trends became readily apparent: for shear layers composed of a supersonic and a subsonic stream, the convective velocity was much faster than the average velocity, thus producing a large M_{c2} and low M_{c1} (fast modes); in shear layers composed of two supersonic streams, the convective velocity was much slower than the average velocity, thus producing a low M_{c2} and large M_{c1} (slow modes). Because the initial region of a supersonic jet consists of a supersonic–subsonic shear layer, the first trend (fast modes) is most relevant here. For the fast modes, the experimental data suggested the following empirical correlation for M_{c2}:

$$M_{c2} = \bar{M}_c + \frac{d_{M_c}}{\sqrt{1 + (a_2/a_1)^2}} \tag{3}$$

where

$$d_{M_c} = \begin{cases} 1.5\bar{M}_c - 0.4, & \bar{M}_c > 0.27 \\ 0, & \bar{M}_c \le 0.27 \end{cases} \tag{4}$$

and

$$\bar{M}_c = \frac{U_1 - U_2}{a_1 + a_2} \tag{5}$$

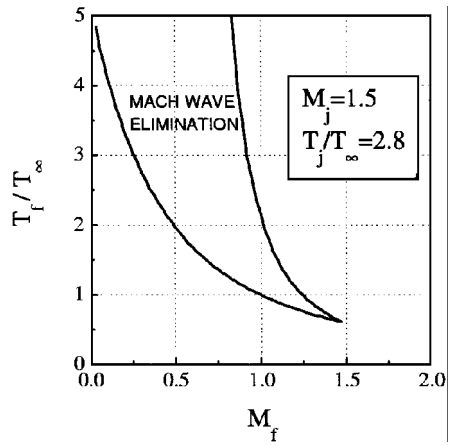

a) $M_\infty = 0$

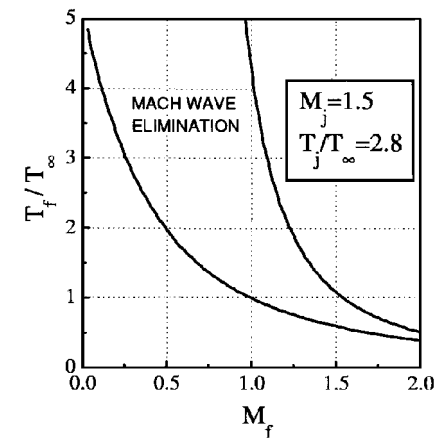

b) $M_\infty = 0.3$

Fig. 3 Model for Mach wave elimination zones.

signifies the symmetric convective Mach number whose value is obtained by setting $M_{c1} = M_{c2}$. The rationale of this correlation is as follows: on the M_{c1} vs M_{c2} plot, the parameter d_{M_c} represents the distance of an experimental measurement from its symmetric value. This distance exhibits a consistent, monotonically increasing trend vs $\bar{M}_c$ [Eq. (4)] and, thus, can be used to predict M_{c1} and M_{c2}. Only the relation for M_{c2} is presented here. The asymmetric behavior of the large eddies is extremely relevant to Mach wave radiation, though the physical mechanisms for the fast modes (and for the slow modes in supersonic–supersonic shear layers) remain elusive.

Using the model of Eqs. (3–5), we can readily derive relations that the coflow static temperature T_f and coflow Mach number M_f must satisfy to prevent Mach wave radiation. They are plotted in Fig. 3 for $M_j = 1.5$, $T_j/T_\infty = 2.8$, and M_∞ taking the values of 0 (static conditions) and 0.3 (typical takeoff speed). The lower bound represents conditions at which $M_{c2_j} = 1$ and the upper bound conditions at which $M_{c2_f} = 1$. One must keep in mind that the relations of Fig. 3 are based on planar shear layers and that the coannular jet may exhibit quite different behavior, especially if the annulus is thin. Therefore, they are used only as a preliminary guide and need to be refined by future experiments. Nevertheless, some important trends are obvious. For subsonic M_f, the coflow generally must be heated for Mach wave elimination to occur. At near-sonic M_f, heating requirements are minimal and possibly zero. As M_f increases, elimination becomes more efficient in terms of heat addition. At the same time, the elimination zone, and hence the operating margin, become narrower. With forward-flight speed, the operating margin is wider but the line $T_f/T_\infty = 1$ presents a lower practical limit (it is unfeasible to cool the coflowing stream in an engine application). An additional practical requirement for the method to work is that the coflow be immediately adjacent to the jet, i.e., there should be no major gaps between the two flows. Gaps would enable generation of Mach waves, thus defeating the purpose of the coflow.

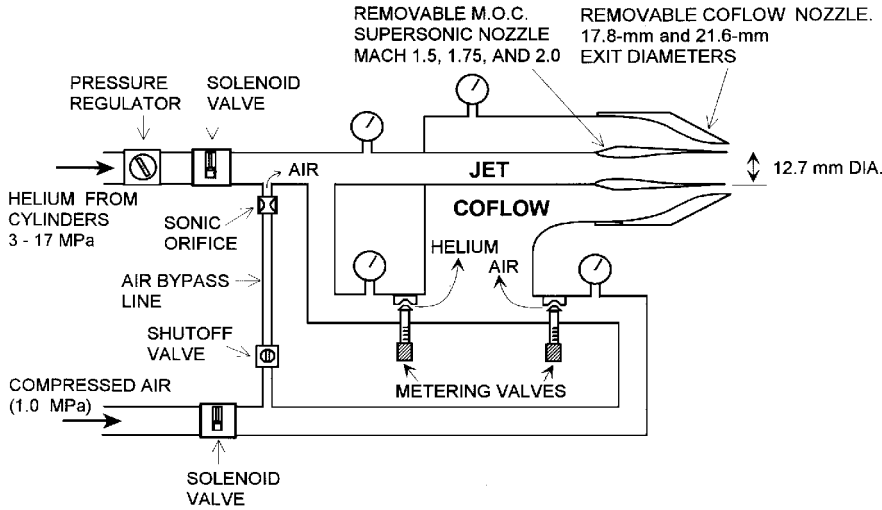

Fig. 4 Coannular supersonic jet facility.

III. Experiment

Experiments were conducted in a new coannular jet facility shown in Fig. 4. Mixtures of helium and air were supplied to a concentric nozzle arrangement accepting a variety of inner and outer nozzles. The inner nozzles, of 12.7-mm exit diameter, were designed by the method of characteristics for Mach numbers 1.5, 1.75, and 2.0. Only the Mach 1.5 results are presented here. The outer nozzles formed smooth contractions terminating in exit diameters of 17.8 and 21.6 mm.

Air was supplied by compressors at a pressure of 1000 kPa (all pressures are absolute). Helium was supplied by 10 high-pressure cylinders and was regulated down to 380 kPa. The supersonic jet consisted of helium mixed with a small amount of air injected to the helium stream through a sonic orifice. The effective diameter of this orifice was determined by flow rate tests to be 3.4 ± 0.1 mm. The purpose of the air injection into the helium stream was to bring the jet velocity and effective temperature down to levels typical of supersonic engine exhausts. The gas mixture was calculated to have a helium mass fraction of 0.56 ± 0.032, gas constant $R = 1300 \pm 70$ J/kgK, and ratio of specific heats $\gamma = 1.55 \pm 0.005$. Part of this mixture was directed to the jet nozzle, and the rest was mixed with pure air and directed to the coflow.

Gas mixing for the coflow stream was controlled by two identical metering valves. The first valve controlled the flow rate of the helium–air mixture (the same mixture that supplied the jet flow), and the second one controlled the flow rate of the pure air. For each valve, the orifice area vs angular position of the valve handle was determined by flow rate tests conducted in house. The accuracy of these tests was 5%, and the results agreed well with the valve manufacturer's specifications. This mixing arrangement enabled accurate control of the density and total pressure of the coflow. A gas dynamic calculation, performed on spreadsheet before each experiment, predicted the helium mass fraction, density, total pressure, Mach number and velocity of the coflow given the metering valve positions, supply pressures of the gases entering the valves, and exit area of the coflow nozzle. Even though it was not possible to independently verify the helium mass fraction, the predicted coflow total pressure matched the experimental value to within 5%. The uncertainty in the metering valve orifice areas, combined with the uncertainty in the composition of the incoming helium–air stream, leads to an uncertainty of 4.5% in the coflow density. The coflow Mach numbers reported here are inferred from the measured total pressures, not the calculated ones, and are accurate to within 1%. The air surrounding the coannular jet was at ambient, still conditions, and the main jet was always perfectly expanded. The coflow was naturally pressured matched at subsonic speeds but was slightly underexpanded at supersonic speeds due to the converging geometry of the coflow nozzle.

In an engine application, the exhaust flow consists of a hot air jet, surrounded by a variable-temperature air coflow, exiting into ambient air. Because the present experiment has no heating capability, the temperature effect is simulated by exhausting helium–air mixtures into ambient air. Of particular importance is to match the density ratios and velocities of the air-to-air jet and coflow. At constant pressure, the density ratio of a hot air-to-air jet is $\rho_\infty / \rho_j = T_j / T_\infty$ It is matched by manipulating the gas constant R of a cold light jet exhausting into ambient air. For ease of reference, the actual light jet is stated to have the same effective temperature as the hot jet, i.e.,

$$(\rho_\infty / \rho_j) = (T_j / T_\infty)_{\text{effective}} = (T_j / T_\infty)_{\text{actual}} (R_j / R_\infty) \qquad (6)$$

The same method is used to manipulate the density ratio of the coflow. All temperatures mentioned hereinafter are effective temperatures, written without subscript. Thus, we have $T_j / T_\infty = \rho_\infty / \rho_j$ and $T_f / T_\infty = \rho_\infty / \rho_f$.

The velocity $U = Ma = M\sqrt{\gamma RT}$ is matched, at least approximately, by manipulating γR, while the Mach number M is the same. When the actual jet and its density-ratio equivalent have different γ, there is a small discrepancy in their velocities at constant Mach number, as pointed out by Kinzie and McLaughlin.[19] In the present study, the speed of the equivalent Mach 1.5 air jet ($\gamma = 1.4$) is 5% lower than the speed of the actual Mach 1.5 helium–air jet ($\gamma = 1.55$), which is reported here. This difference is deemed too minor to affect the results.

A pitot probe recorded the centerline pitot pressure, which was translated to Mach number via the Rayleigh pitot formula. Because the jet flow is mixed with the coflow and with the ambient air, a value of $\gamma = 1.5$ was used in the Rayleigh pitot formula, i.e., a value between the jet exit and ambient γ. The sensitivity of this Mach number on the choice of γ is very small. As an example, for a pitot-to-static pressure ratio of 2.5, the Mach number is 1.23 for $\gamma = 1.4$, 1.20 for $\gamma = 1.5$, and 1.18 for $\gamma = 1.55$.

Schlieren photography was used to detect the Mach waves. The schlieren system employs a 20-ns spark source (Xenon Nanolamp®) for fast photography. The knife-edge orientation was aligned with the expected slope of the Mach waves to accentuate them on the images. A pinhole was also used occasionally. The images were recorded on a digital charge-coupled-device camera (Photometrics Star I) with 12-bit, 384×576 array. The automated facility was instrumented with pressure transducers recording the total pressures in the jet and coflow as well as the pitot pressure. Table 1 presents the range of flow conditions covered in the Mach 1.5 jet experiments.

IV. Image Processing

Figure 5 shows a comparison between the untreated Mach 1.5 jet (no coflow) and the same jet surrounded by coflow of diameter ratio $D_f / D_j = 1.7$ and with $M_f = 1.15$ and $T_f / T_\infty = 1.0$ conditions near the tip and inside the predicted Mach wave elimination zone of Fig. 3a. It is seen that the coflow treatment removes the Mach waves. We obtain a more detailed view of the waves and their elimination by enhancing the images according to the scheme that follows.

Table 1 Flow conditions

Quantity	Value	Uncertainty, %
Jet Mach number	1.5	1.0
Coflow Mach number	0–1.2[a]	1.0
Helium mass fraction in jet	0.56	5.6
Helium mass fraction in coflow	0–0.28	6.3
Jet velocity, m/s	920	3.0
Coflow velocity, m/s	0–500	2.6
Jet effective temperature, K	840	4.9
Coflow effective temperature, K	250–700	4.5
Jet diameter, mm	12.7	0.0
Coflow diameters, mm	17.8, 21.6	0.0
Jet Reynolds number	3.8×10^5	10

[a]Underexpanded for $M > 1$.

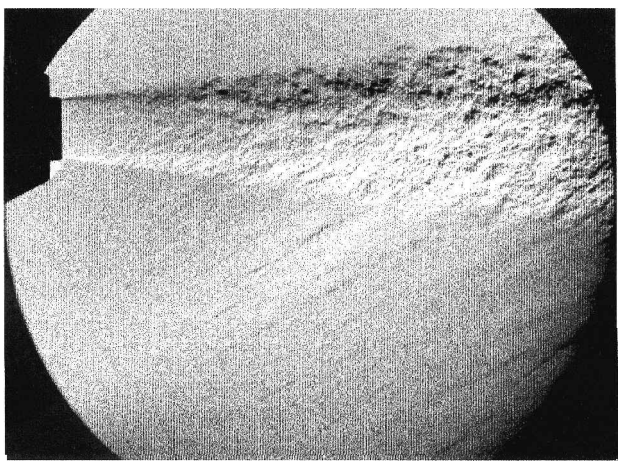

a) Untreated jet

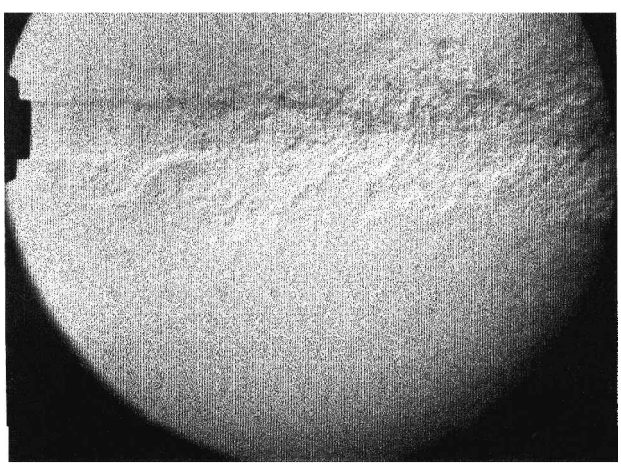

b) Treated jet with $M_f = 1.15$ and $T_f/T_\infty = 1.0$

Fig. 5 Unprocessed schlieren images.

The purpose of the digital image enhancement was to accentuate the waves in the ambient air, rather than the turbulent structure of the jet, and to do so in an automated, consistent fashion for all of the images. To explain the processing scheme, we denote an image by the matrix $A(x, y)$, where x and y are integers. First, the image undergoes median filtering with a large, 31×31 matrix. Unlit regions of the image are excluded from this and all subsequent filtering operations. The resulting image, $\bar{A}(x, y)$, is then subtracted from the original to give the fluctuation image

$$A\prime(x, y) = A(x, y) - \bar{A}(x, y)$$

The fluctuation image has completely uniform background, unlike the original image whose background variations are inevitable (especially at high contrast) because the spark is not a perfect point or line source. The global maximum and minimum of the fluctuation image, $A\prime_{\max}$ and $A\prime_{\min}$, are then computed. These extrema depend to a large extent on the density variations in the jet. By using them to scale the image, as shown next, a degree of consistency is achieved in interpreting all of the processed images.

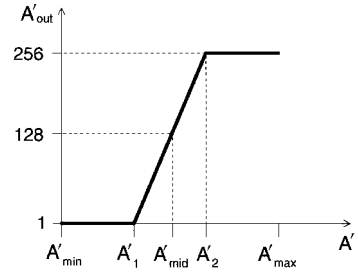

Fig. 6 Image processing scheme for the fluctuation image $A\prime(x, y)$.

To accentuate the features within a certain intensity range of $A\prime(x, y)$, the linear ramp algorithm of Fig. 6 is used to construct the output image. The slope of the ramp, defined by its start- and endpoints $A\prime_1$ and $A\prime_2$, determines the sensitivity

$$S = 1 - \frac{A\prime_2 - A\prime_1}{A\prime_{\max} - A\prime_{\min}} \tag{7}$$

which lies in the range $0 \leq S < 1$, zero being the least sensitive. The location of the midpoint of the ramp, $A\prime_{\text{mid}}$, determines which range of intensities get accentuated. To emphasize the Mach waves, $A\prime_{\text{mid}}$ was set equal to the mean value of $A\prime$ in an image subregion outside the jet. The 8-bit output image is constructed according to

$$A\prime_{\text{out}}(x, y) = 1 + 255\frac{A\prime(x, y) - A\prime_1}{A\prime_2 - A\prime_1} \tag{8}$$

valid in the range $A\prime_1 \leq A\prime \leq A\prime_2$. Outside that range, $A\prime_{\text{out}} = 1$ for $A\prime < A\prime_1$ and $A\prime_{\text{out}} = 256$ for $A\prime > A\prime_2$. The image processing algorithm was written in Fortran. All of the images of this study were processed with sensitivity $S = 0.85$. Processing was fully automated, requiring no further user input.

V. Results

Figure 7 shows the enhanced versions of the images in Fig. 5. The bypass ratio $B = \dot{m}_f/\dot{m}_j$ and the thrust ratio TR (thrust of treated jet over thrust of untreated jet) are shown in the labels. Enhancement helps bring out interesting features of the pressure waves that might otherwise go unnoticed. Note that the schlieren knife edge was oriented to emphasize waves in the lower part of the jet; as a result, turbulent features appear different in the upper and lower edges of the jet. In the untreated case, the waves emitted by the supersonic eddies (Mach waves) are seen as straight (conical) with nearly constant slope, indicating that there is a single convective velocity for the large eddies in the shear layers surrounding the potential core. The slope of the Mach waves is approximately 30 deg, from which we obtain $M_{c2_j} \approx 2.0$; thus, $U_{c_j}/U_j \approx 0.75$. The model of Eqs. (3–5) predicts $M_{c2_j} = 1.9$. The convective velocity observed here is similar to the phase speeds of the axisymmetric (for low Strouhal number) and helical (for high Strouhal number) Kelvin–Helmholtz instability computed by Seiner et al.[5] for hot supersonic round jets.

Careful examination of the image also reveals the existence of weaker waves of a different family: circular (spherical), originating from near the lip of the inner nozzle. They are emitted from a stationary source, in contrast to the Mach waves, which are emitted by moving sources, from the eddies. The coexistence of the two families of waves is illustrated by the sketch of Fig. 8. To try to understand the source of the spherical waves, the helium–air mixture in the jet flow was substituted by air at the same pressure ratio. Spherical waves were not observed in the air jets. Therefore, it is unlikely that they were caused by any disturbances originated in the piping system. Instead, they were likely created by vortex shedding at the nozzle lip, which is much stronger in light jets due to their faster growth rate. Similar wave phenomena have been observed in supersonic helium jets injected transversely to a supersonic airstream.[20]

Application of the coflow in Fig. 7 removes both the Mach waves and the weaker spherical waves. The air surrounding the jet appears much quieter, even though the combination of jet plus coflow generates 90% more thrust than the sole jet. Elimination here is achieved with an unheated coflow at slightly supersonic conditions.

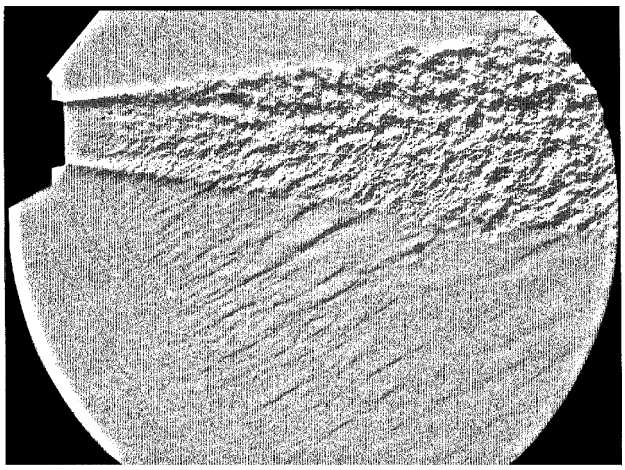

a) Untreated

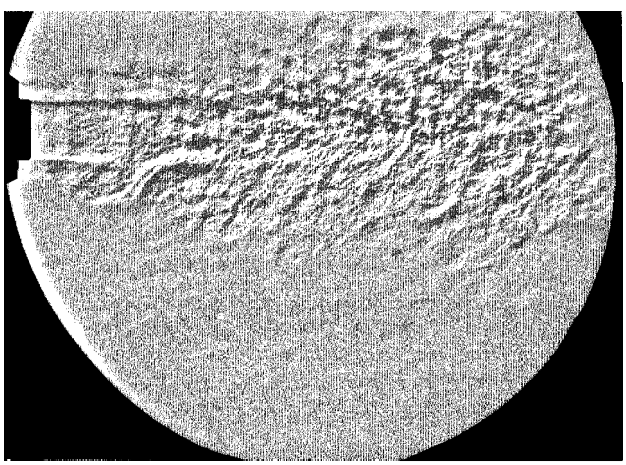

b) Treated with $M_f = 1.15$, $T_f/T_\infty = 1.0$, $B = 2.0$, and $TR = 1.9$

Fig. 7 Processed schlieren images of jet with coflow diameter D_f/D_j = 1.7.

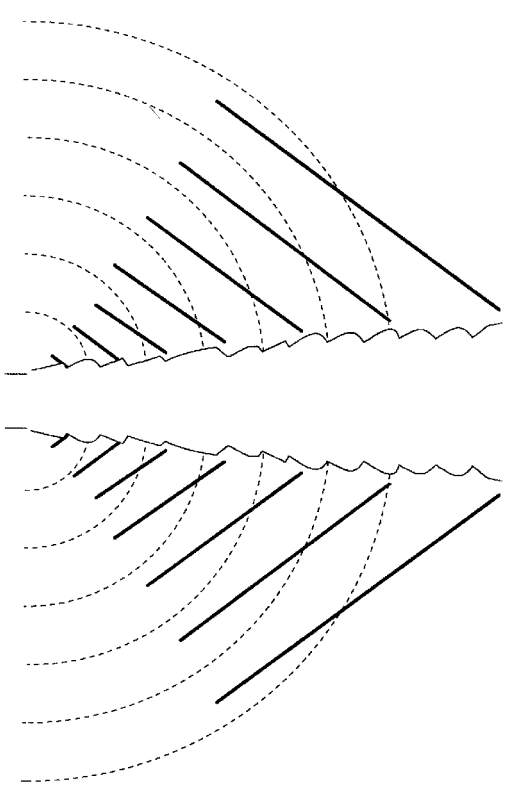

Fig. 8 Waves from ——, moving sources and – – –, stationary sources.

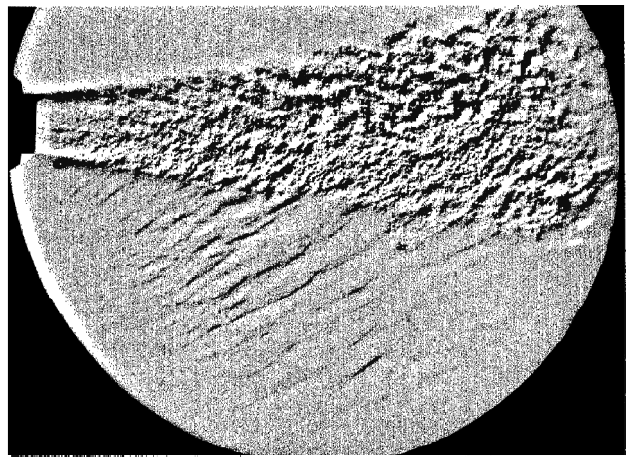

a) Untreated

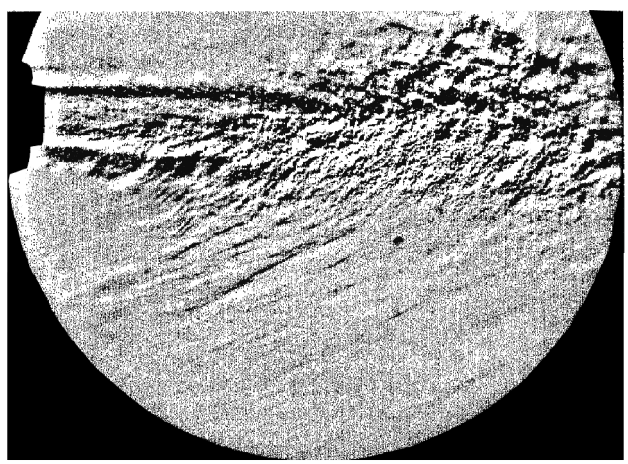

b) Improperly treated with $M_f = 0.75$, $T_f/T_\infty = 1.0$, $B = 1.5$, and $TR = 1.4$

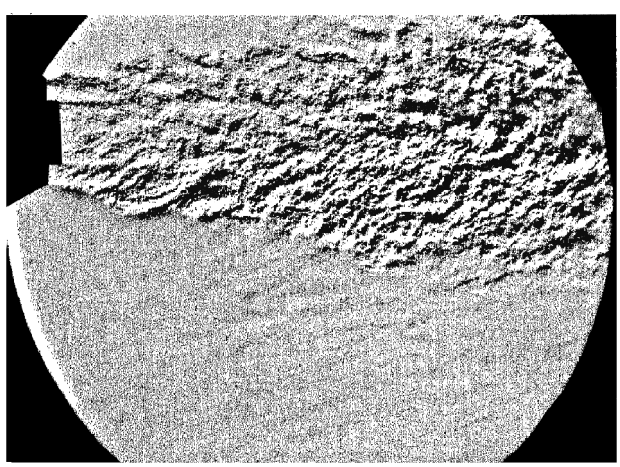

c) Properly treated with $M_f = 0.75$, $T_f/T_\infty = 2.0$, $B = 1.1$, and $TR = 1.5$

Fig. 9 Additional processed images of jet with coflow diameter D_f/D_j = 1.7.

Figure 9 shows another elimination sequence: untreated, improperly treated, and properly treated. In Fig. 9b, the coflow is supplied at conditions outside the predicted elimination region; accordingly, Mach waves develop. The coflow of Fig. 9c is supplied at conditions inside the elimination region, with high effective temperature and subsonic Mach number; as predicted, Mach waves disappear. Figure 10 shows a treatment sequence for a jet with small coflow diameter, $D_f/D_j = 1.4$. This very thin coflow layer provides substantial elimination, but typically a few weak waves remain. It is expected that a thin coflow gets consumed faster by entrainment and hence is less effective in eliminating Mach waves than a thick one. Still, the extent to which this thin coflow works is surprising and is discussed more in Sec. VI.

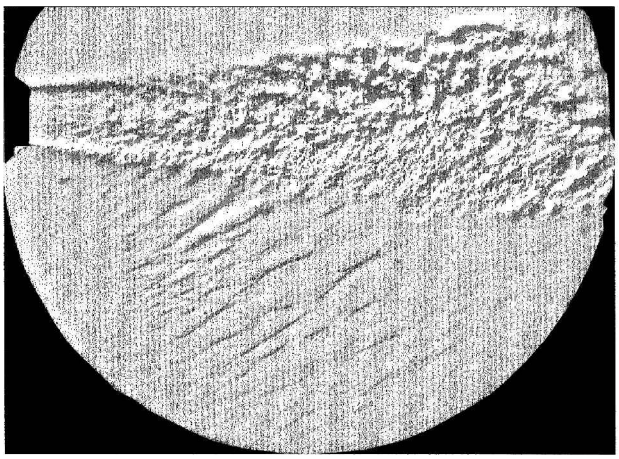

a) Untreated

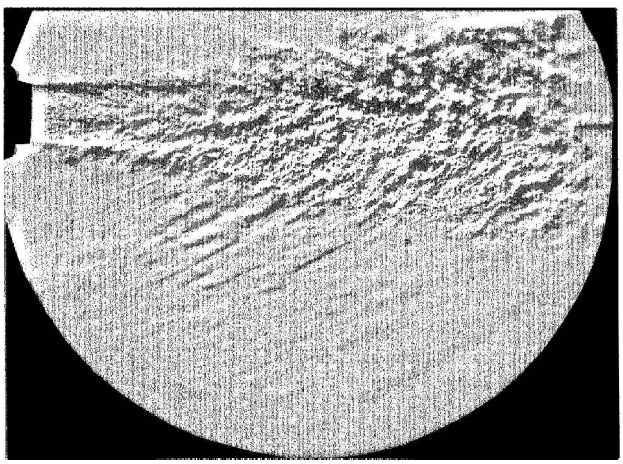

b) Improperly treated with $M_f = 0.75$, $T_f/T_\infty = 1.0$, $B = 0.8$, and $TR = 1.3$

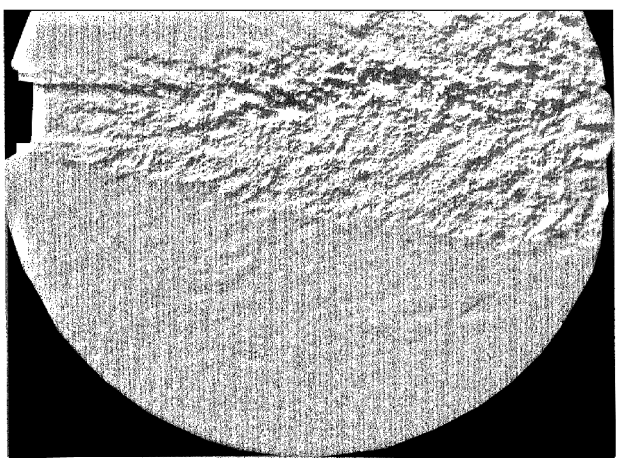

c) Properly treated with $M_f = 1.15$, $T_f/T_\infty = 1.1$, $B = 1.1$, and $TR = 1.6$

Fig. 10 Processed images of jet with coflow diameter $D_f/D_j = 1.4$.

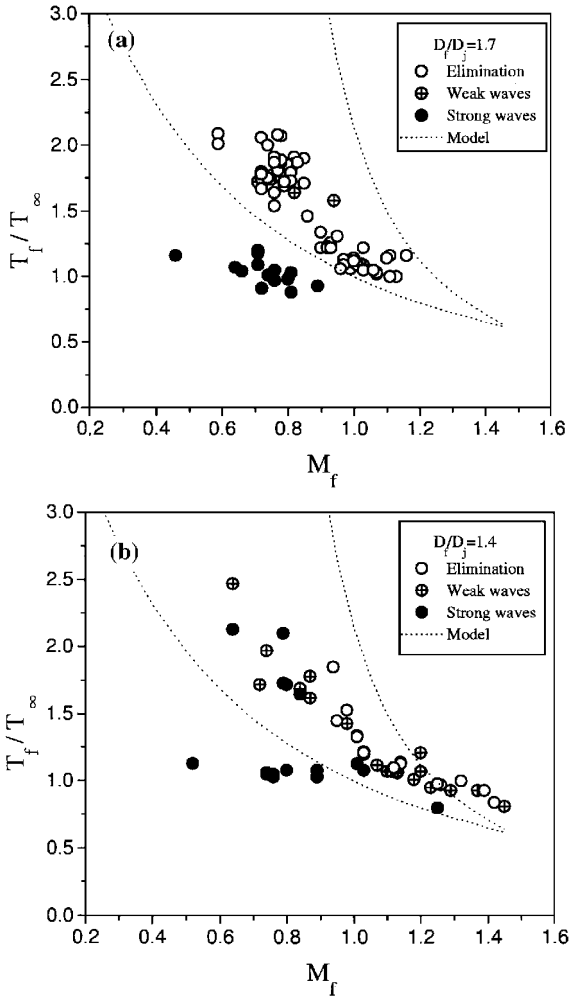

Fig. 11 Experimental data of Mach wave elimination.

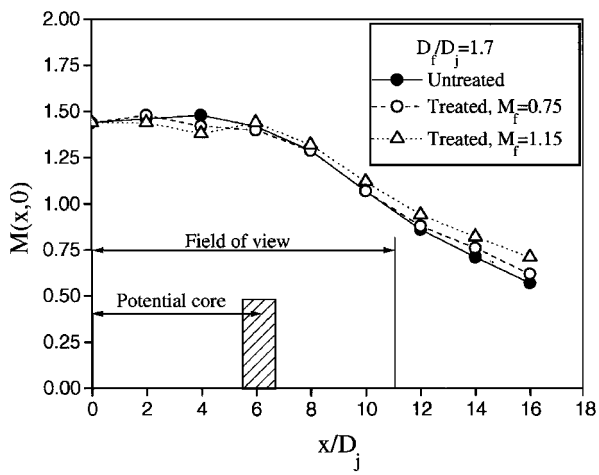

Fig. 12 Centerline Mach number distributions.

The schlieren results are summarized on the T_f vs M_f diagrams of Fig. 11. The images were divided into three classes: elimination denotes a very clean image devoid of any discernible Mach waves, as in Fig. 7b; weak waves signify the presence of very few weak Mach waves, as in Fig. 10c; strong waves mean Mach waves of strength similar to those of the untreated jet, as in Fig. 9b or 10b. For the larger coflow diameter (Fig. 11a), the experimental region of elimination is in good agreement with the prediction of Fig. 3a. Inside this region, the vast majority of images indicate complete elimination, with very few images showing weak waves. Outside the region, strong waves were apparent. For the smaller coflow diameter (Fig. 11b), strong waves sometimes appeared inside the predicted elimination zone at subsonic M_f. This intermittent weakening of the coflow effectiveness is probably due to its entrainment by the main jet. At higher M_f, agreement with the predicted elimination zone is fair, though a few weak waves remained occasionally.

In addition to suppressing Mach wave radiation, one is also interested in rapidly decelerating the jet flow to subsonic speeds so that other sources of turbulent noise are minimized. Thus, it is important to establish the effect of the coflow on the centerline velocity decay. Axial pitot surveys were performed, from which the centerline Mach number distribution was calculated assuming an average $\gamma = 1.5$. The centerline Mach number distributions for untreated and treated cases is presented in Fig. 12, where it is seen that the

coflow has minimal impact on the Mach number decay. Scaled for the higher thrust of the combined flow, the coflow treatment effectively enhances the Mach number decay. For example, the treated jet with $M_f = 1.15$ produces 1.9 times the thrust of the untreated jet. The same thrust would have been produced by an untreated jet with effective diameter $D_{\text{eff}} = \sqrt{1.9} D_j = 1.37 D_j$. The Mach number decay of this larger untreated jet is obtained by stretching axially the untreated line of Fig. 12 by a factor of 1.37. In that case, the decay rate of the treated jet is faster than that of the larger untreated jet.

The pitot measurements indicate that the potential core ends within $x/D_j = 6$, which is approximately one-half of the field of view of the images presented. The corresponding shear layer growth rate is 0.17, or 10 deg, in agreement with visual observations. The source of Mach wave radiation spans from the jet exit to 1–2 diameters past the end of the potential core. Images of untreated jets in the region $11 < x/D_j < 22$ do not show Mach wave radiation; consequently, no significant differences are seen between treated and untreated jets in that region.

VI. Practical Applications

The turbofan engine is a natural candidate for implementation of the Mach wave elimination technique inasmuch as a coflowing stream already exists in the form of the fan stream. There is a multitude of ways in which the technique could be applied, from modifying existing designs to creating new ones. Precise cost-benefit figures depend strongly on the details of the implementation and are beyond the means of this investigation. The purpose of this section is to provide a preliminary performance estimate that may form the basis for more refined calculations in the future.

The results of the present study (Fig. 11), coupled with practical design considerations, suggest two limits in the range of options available in applying Mach wave elimination to a turbofan engine: 1) unheated fan stream with low-supersonic exhaust Mach number produced by a fan pressure ratio of around 2.5 and 2) heated fan stream with moderate exhaust Mach number produced by a fan pressure ratio of around 1.5. Heating may be achieved by burning fuel in the duct, injecting hot air from the core combustor, or other means.

Operation near limit 1 appears more attractive because it does not require heating of the fan stream and may even result in better propulsive efficiency due to the higher bypass ratio. Operation near limit 2 is less efficient but may be more easily implemented in existing designs because it requires a fan pressure ratio achievable with a single stage of blades. Inasmuch as it involves only heat addition to the fan stream, all other parameters staying fixed, it is also the easiest condition to analyze. Next we obtain a preliminary performance estimate for an engine operating near limit 2.

We consider an engine with fan pressure ratio of 1.5 (unheated $M_f = 0.8$ and $U_f = 280$ m/s) and bypass ratio of 1.0 exhausting into ambient, still conditions ($T_\infty = T_{0_\infty} = 300$ K). In the notation that follows, primed quantities are those affected by treatment. Note that the presumed isentropic fan compression raises the fan total temperature to $T_{0f} = 1.12 T_{0_\infty}$. The core jet properties are given in Table 1. Untreated, the flow would resemble that of Fig. 9b, i.e., Mach waves would be emitted. Supposing that we apply treatment according to Fig. 9c, the coflow temperature ratio must be $T_f'/T_\infty = 2.0$. The corresponding total–temperature ratio is $T_{0_f}'/T_{0_f} = 2.0$. If heat is added to the fan stream at low Mach number, total-pressure losses are small and it can be shown that the fan slipstream velocity increases according to $U_f'/U_f = \sqrt{(T_{0_f}'/T_{0_f})}$, i.e., fan velocity increases here by 41%.

The additional mass flow rate of kerosene required to raise the fan total temperature from T_{0_f} to T_{0_f}' is

$$\Delta \dot{m}_k = \frac{\dot{m}_f c_p (T_{0_f}' - T_{0_f})}{Q_k} \tag{9}$$

where $\dot{m}_f$ is the fan mass flow rate, c_p the specific heat for air, and Q_k the heating value for kerosene. The modified thrust specific fuel consumption (TSFC) for the entire engine is

$$\text{TSFC}' = \frac{\dot{m}_k + \Delta \dot{m}_k}{\text{total thrust}} = \text{TSFC} + \frac{\Delta \dot{m}_k}{\dot{m}_j U_j + \dot{m}_f U_f'} \tag{10}$$

Substituting Eq. (8), and normalizing by the unmodified TSFC, we obtain

$$\frac{\text{TSFC}'}{\text{TSFC}} = 1 + \left[\frac{c_p T_{0_f}}{\text{TSFC}\, Q_k U_j}\right]\left[\frac{B}{1 + B U_f'/U_j}\right]\left[\frac{T_{0_f}'}{T_{0_f}} - 1\right] \tag{11}$$

where $B = \dot{m}_f/\dot{m}_j$ is the bypass ratio. Substituting the values $c_p = 1$ kJ/kg K, $Q_k = 42{,}000$ kJ/kg (= 19,000 Btu/lbm), TSFC = 1/70,600 kg/s/N (= 0.5 lbm/h/lbf), $U_j = 920$ m/s, $U_f' = 400$ m/s, $T_{0_f} = 340$ K, and $B = 1.0$, we obtain TSFC′/TSFC = 1.42. Heat addition will be applied for only short intervals, takeoff and possibly landing, of a long flight. Assuming it is activated for a total of 3 min in a 180-min flight, then the effective TSFC ratio is TSFC′/TSFC = 1 + (0.42)(3)/180 = 1.007. In other words, impact on overall fuel consumption is on the order of 0.5%. It is noted again that this is a preliminary estimate on one of the less-efficient treatment options. The 41% increase in fan exhaust velocity causes the same increase in fan thrust. Here, fan thrust accounts for 31% of the total thrust, and so total thrust increases by 12%.

In applying the Mach wave elimination technique to an engine, we must be aware of additional issues that may affect the acoustic performance. Operation near limit 1 will probably require a two-stage fan; the possible increase in fan noise must be taken into account when evaluating the technique. Operation near limit 2, which requires heating of the fan stream, may introduce combustion noise in that stream. These are issues that must be addressed in large-scale tests using realistic models of jet engines.

VII. Concluding Remarks

This research has shown that application of an annular coflow around a pressure-matched supersonic jet can significantly alter the pressure field of the jet. At the proper conditions, the coflow eliminates Mach wave radiation and hence removes a strong source of noise from the flow. Most importantly, the experiments have demonstrated that Mach wave elimination can occur at conditions that are practically and economically feasible from a propulsion standpoint. Applied to a typical turbofan engine, this noise suppression technique is estimated to increase takeoff thrust, with very small impact on overall fuel consumption.

Although Mach wave elimination was achieved at conditions close to those predicted, it is still surprising that the effect of the coflow, especially of the thin one, persisted so far downstream. Given the 10-deg spreading rate of the shear layers, it was expected that a coflow of 2.5 mm thickness would be fully entrained within a length of 29 mm, i.e., within two jet diameters. For the 4.4-mm-thick coflow the corresponding figure is 4 jet diameters. Yet, in both cases Mach waves were eliminated in a region spanning about 11 jet diameters. Moreover, the growth rate of the jet did not change appreciably. Therefore, we must investigate whether, in addition to the expected benefits, the coflow produces subtle but important changes to the turbulent structure. One possibility is that the coflow, injected at high M_f, reduces the convective velocity of the jet eddies, something counterintuitive but in accordance with the slow modes of U_c seen in supersonic–supersonic shear layers.[14,18]

The impetus, and ultimate goal, of this research is supersonic jet noise reduction without mechanical suppressors. However, the Mach wave elimination may also benefit the current mixer–ejector concept in the form of alleviating acoustic loads on the inner ejector surface. Another related application could be reduction of acoustic loads on aircraft structures exposed to Mach wave radiation from engine exhaust. Our experiments will continue with microphone surveys of the acoustic field of the jet and with direct measurements of the convective velocities of the large eddies.

Acknowledgments

The support by NASA Langley Research Center is gratefully acknowledged (Grant NAG-1-1729; John M. Seiner, Program Monitor). Many thanks to Michael B. Ryan for his assistance with the construction of the jet facility. The method described herein has been granted a United States Patent, No. 5,590,520.

References

[1]McLaughlin, D. K., Morrison, G. D., and Troutt, T. R., "Experiments on the Instability Waves in a Supersonic Jet and Their Acoustic Radiation," *Journal of Fluid Mechanics*, Vol. 69, No. 11, 1975, pp.73–95.

[2]Troutt, T. R., and McLaughlin, D. K., "Experiments on the Flow and Acoustic Properties of a Moderate Reynolds Number Supersonic Jet," *Journal of Fluid Mechanics*, Vol. 116, March 1982, pp. 123–156.

[3]Tam, C. K. W., and Burton, D. E., "Sound Generated By Instability Waves of Supersonic Flows. Part 2. Axisymmetric Jets," *Journal of Fluid Mechanics*, Vol. 138, Jan. 1984, pp. 249–271.

[4]Tam, C. K. W., Chen, P., and Seiner, J. M., "Relationship Between Instability Waves and Noise of High-Speed Jets," *AIAA Journal*, Vol. 30, No. 7, 1992, pp. 1747–1752.

[5]Seiner, J. M., Bhat, T. R. S., and Ponton, M. K., "Mach Wave Emission from a High-Temperature Supersonic Jet," *AIAA Journal*, Vol. 32, No. 12, 1994, pp. 2345–2350.

[6]Mitchell, B. E., Lele, S. K., and Moin, P., "Direct Computation of the Sound Generated by Subsonic and Supersonic Axisymmetric Jets," Thermosciences Div., Dept. of Mechanical Engineering, Rept. TF-66, Stanford Univ., Stanford, CA, Nov. 1995.

[7]Seiner, J. M., and Krejsa, E., "Supersonic Jet Noise and the High Speed Civil Transport," AIAA Paper 89-2358, Jan. 1989.

[8]Nagamatsu, H. T., Sheer, R. E., and Gill, M. S., "Characteristics of Multitude Multishroud Supersonic Jet Noise Suppressor," *AIAA Journal*, Vol. 10, No. 3, 1972, pp. 307–313.

[9]Papamoschou, D., "Analysis of Partially-Mixed Supersonic Ejector," *Journal of Propulsion and Power*, Vol. 12, No. 4, 1996, pp. 736–741.

[10]Tillman, T. G., Paterson, R. W., and Presz, W. M., "Supersonic Nozzle Mixer Ejector," *Journal of Propulsion and Power*, Vol. 8, No. 2, 1992, pp. 513–519.

[11]Tanna, H. K., "Coannular Jets—Are They Really Quiet and Why?," *Journal of Sound and Vibration*, Vol. 72, No. 1, 1980, pp. 97–118.

[12]Dosanjh, D. S., Yu, J. C., and Abdelhamid, A. N., "Reduction of Noise from Supersonic Jet Flows," *AIAA Journal*, Vol. 9, No. 12, 1971, pp. 2346–2353.

[13]Majjigi, R. K., Brausch, J. F., Janardan, B. A., Balsa, T. F., Knott, P. R., and Pickup, N., "Free Jet Feasibility Study of a Thermal Acoustic Shield Concept for AST/VCE Application," NASA CR-3758, 1984.

[14]Papamoschou, D., "Structure of the Compressible Turbulent Shear Layer," AIAA Paper 89-0126, Jan. 1989.

[15]Fourguette, D. C., Dibble, R. W., and Mungal, M. G., "Time Evolution of the Shear Layer of a Supersonic Axisymmetric Jet at Matched Conditions," *AIAA Journal*, Vol. 29, No. 7, 1991, pp. 1123–1130.

[16]Hall, J. L., Dimotakis, P. E., and Rosemann, H., "Experiments in Non-Reacting Compressible Shear Layers," *AIAA Journal*, Vol. 31, No. 12, 1993, pp. 2247–2254.

[17]Nagai, M., "Mechanism of Pseudo-Shock Wave in Supersonic Jet," *Bulletin of the Japan Society of Mechanical Engineers*, Vol. 26, No. 212, 1983, pp. 207–211.

[18]Papamoschou, D., and Bunyajitradulya, A., "Evolution of Large Eddies in Compressible Shear Layers," *Physics of Fluids*, Vol. 4, No. 3, 1997, pp. 756–765.

[19]Kinzie, K. W., and McLaughlin, D. K., "An Experimental Study of Noise Radiated from Supersonic Elliptic Jets," AIAA Paper 95-0511, Jan. 1995.

[20]Papamoschou, D., and Hubbard, D. G., "Visual Observations of Supersonic Transverse Jets," *Experiments in Fluids*, Vol. 14, No. 6, 1993, pp. 468–471.

F. W. Chambers
Associate Editor